CEAS-GNC-2022-072

CEAS EuroGNC 2022
"Conference on Guidance, Navigation and Control"
3-5 May 2022 @ Technische Universität Berlin, Germany

Data-efficient capture region estimation for tactical missile using active sampling based Gaussian process classification

Youngjun Lee Ph.D. candidate, Seoul National University, Department of Aerospace engineering, 08826, Seoul, Republic of Korea. josj80@sun.ac.kr

Sangmin Lee Ph.D. candidate, Seoul National University, Department of Aerospace engineering, 08826, Seoul, Republic of Korea. everlastingminii@gmail.com

Youdan Kim Professor, Institute of Advanced Aerospace Technology, Department of Aerospace Engineering, 08826, Seoul, Republic of Korea. ydkim@snu.ac.kr

ABSTRACT

An efficient capture region estimation algorithm is proposed for a missile. The Gaussian process classifier and active sampling technique are combined to improve the accuracy of the predictive model while efficiently using data. The key idea is to actively sample the data required for the learning method, which uses the information on the uncertainty predicted from the Gaussian process classifier. Data necessary for training are obtained using a planar missile simulator, and impact-angle control composite control guidance is used for intercepting the target while satisfying the impact angle requirement. Through numerical simulation, it is shown that the accuracy of the trained model gradually increases during training progress, and the performance of the finally-trained predictive model is verified. It is also shown that the efficiency of the data usage and the accuracy of the trained model are relatively better than a Gaussian process classifier trained without active sampling.

Keywords: Gaussian Process Classification; Active Sampling, Capture Region Estimation, Impact Angle Control Composite Guidance

Nomenclature

f	=	The latent function
p	=	The size of input space
n	=	The number of training data
n_t	=	The number of test data
$\mathbb{X}$	=	Input space
μ	=	Expectation function
k	=	Kernel function
σ_f	=	Signal standard deviation
$\sigma_1, \ldots, \sigma_n$	=	Length-scale
$\mathscr{L}$	=	Given dataset
a_M	=	Normal acceleration

ψ = Vector of hyperparameters
γ_M = The flight path angle of missile
γ_T = The flight path angle of target
γ_{M_f} = The flight path angle of missile at impact
λ = Line-of-sight (LOS) angle
r = Relative distance between missile and target
V_M = Speed of missile
V_T = Speed of target
σ_{lim} = Field-of-view limit of seeker
G = Look angle gain
N = Navigation constant
λ_s = Switching LOS angle
η = The speed ratio of missile and target
σ_d = The desired look angle

1 Introduction

Recently, research on the reachability analysis of tactical missiles has been drawing much attention. Since missiles cannot always successfully intercept the target due to various constraints, a set of initial conditions capable of intercepting a target called a capture region should be determined. Obtaining an accurate capture region is crucial in determining the performance of the missile system. According to recent research trends, guidance laws that can achieve additional requirements such as impact angle and time control have been studied [1–4]. Consideration of practical constraints such as the field-of-view limit of missiles has also been addressed [5, 6], and maneuvering target has also been considered [7, 8]. As the additional mission requirements and physical constraints of the missiles are added, the capture region becomes narrowed. The narrower the capture region of the missile, the more critical the accurate estimation of the capture regions becomes.

There are two approaches to estimating the capture regions. First, capture regions are computed analytically using a theoretical approach. For example, the capture regions for planar engagement scenarios were derived through a theoretical methodology [9, 10]. However, these methodologies have clear limitations. Capture regions obtained analytically may be inaccurate in a real engagement environment. Note that it is impossible to analyze the capture region considering all of the uncertain factors in real-world engagement, such as aerodynamic uncertainties or disturbances. As an alternative, the capture region can be estimated through numerical simulation. This method determines successful interception regions by using a high fidelity simulator and performing simulations for all initial conditions of interest. If the reliability of the simulator is guaranteed, then it is possible to estimate the capture region accurately. However, this approach requires a significant amount of computation. In general, the higher the reliability of the simulator, the much more calculations are required to perform the simulation.

Studies related to the design of a predictive model estimating the capture regions based on data have been conducted to overcome these shortcomings. In [11], a predictive model was designed to obtain a probability of successful interception using an artificial neural network. In [12], the capture region of the proportional navigation guidance law was computed using a support vector machine technique. In these studies, capture regions are estimated by applying supervised learning techniques. Note that a artificial neural network is one of the strong candidates among supervised learning algorithms, but unfortunately, it usually requires a considerable amount of data. Therefore, a method ensuring accuracy with fewer data usage is needed.

This study proposes a methodology for estimating capture regions using the data more efficiently. To this end, an algorithm combining the Gaussian process classification and the active sampling is proposed

to use as little data as possible. Active sampling is adopted, which obtains an accurate model using fewer data by automatically selecting data in areas where the model's predictive power is uncertain. The active sampling algorithm actively determines and selects the data required to improve the performance of a given predictive model [13].

The Gaussian process classifier is trained with some of the data generated by numerical simulation. Then, the performance of the proposed technique is analyzed by separating it into learning data and test data. For comparison, the actual capture region data is obtained by performing many numerical simulations. Compared to the method without using active sampling, it was confirmed that the proposed method showed satisfactory performance using fewer data.

This paper is organized as follows. Section 2 mainly explains the theoretical background of Gaussian process classification techniques and active sampling. Section 3 describes the engagement scenario considered in this study and the guidance law to obtain the capture region. Section 4 presents the results of calculating the capture region, followed by the analysis of the results. Finally, we provide the concluding remarks of this study.

2 Theoretical Background

In this section, the theoretical background is briefly introduced for designing a Gaussian process classifier (GPC) with active sampling (AS).

2.1 Gaussian Process Classification

Gaussian process classification model can be briefly described as

$$p(f) = GP(f, \mu, k) \tag{1}$$

where f is a latent function, $\mu : \mathbb{X} \to \mathbb{R}$ is an expectation function, $k : \mathbb{X} \times \mathbb{X} \to \mathbb{R}^{n \times n}$ is a kernel function, and $\mathbb{X} \subset \mathbb{R}^p$ is input space. For any inputs $X = [\mathbf{x}_1 \dots \mathbf{x}_n]$, $\mathbf{x}_i \in \mathbb{X}$, $\mathbf{f} = [f(\mathbf{x}_1) \dots f(\mathbf{x}_n)]^T$ is assumed to follow a multivariate Gaussian distribution with $\mu = [\mu(\mathbf{x}_1), \mu(\mathbf{x}_2), ..., \mu(\mathbf{x}_n)]^T$ as an expectation vector and K as a covariance matrix, where K is n by n matrix whose (i, j) element is $k(\mathbf{x}_i, \mathbf{x}_j)$. To design a classification model, a relationship between the latent variable and the output variable is determined by a nonlinear function σ called the link function as

$$p(y|\mathbf{x}, f) = \sigma(yf) \tag{2}$$

where $\mathbf{x} \in \mathbb{R}^p$, $y \in \{-1, 1\}$, and $\sigma : \mathbb{R} \to [0, 1]$. σ is a function that satisfies the following property; $\sigma(x) = 1 - \sigma(-x)$.

2.2 Design parameters

2.2.1 Expectation and kernel function

Given training data, mean function, kernel function, and link function should be determined. In this study, zero mean function and exponential kernel are used as

$$\mu(\mathbf{x}) \equiv 0 \tag{3}$$

$$k(\mathbf{x}, \mathbf{x}') = \sigma_f^2 \exp(-\frac{1}{2}(\mathbf{x} - \mathbf{x}')^T M(\mathbf{x} - \mathbf{x}')) \tag{4}$$

where $\mathbf{x}, \mathbf{x}' \in \mathbf{X}$, $\sigma_f \in \mathbb{R}$, and $M \in \mathbb{R}^{p \times p}$,with $M_{ii} = \sigma_i \in \mathbb{R}$. σ_f and σ_i deonte signal variance and length-scale, respectively.

2.2.2 Link function

The classification model requires a nonlinear function with a paricular property called the link function. In this study, the following cumulative Gaussian distribution function is used.

$$\sigma(x) = \Phi\left(\frac{x-\mu}{\zeta}\right) = \frac{1}{2}\left[1 + \mathrm{erf}\left(\frac{x-\mu}{\zeta\sqrt{2}}\right)\right] \tag{5}$$

where ζ is standard deviation of a Gaussian random variable and

$$\Phi(x) = \frac{1}{2}\left[1 + \mathrm{erf}\left(\frac{x}{\sqrt{2}}\right)\right] \tag{6}$$

$$\mathrm{erf}(x) = \frac{2}{\sqrt{\pi}}\int_0^x e^{-t^2} dt \tag{7}$$

2.3 Inference

The procedure for obtaining the probability of success in Gaussian process classification is as follows. First, a posterior distribution of latent variables is required. Then, the success probability prediction model is calculated using the obtained posterior distribution and link function. According to the characteristics of the Gaussian process, the joint distribution of the training output and the test output follows a multivariate Gaussian distribution, and the expected value and covariance can be determined as

$$\begin{bmatrix} \mathbf{f} \\ \mathbf{f}_* \end{bmatrix} = \mathcal{N}\left(\begin{bmatrix} \mu \\ \mu_* \end{bmatrix}, \begin{bmatrix} K & K_* \\ K_*^T & K_{**} \end{bmatrix}\right) \tag{8}$$

where $\mu = [\mu(\mathbf{x}_1), \mu(\mathbf{x}_2), ..., \mu(\mathbf{x}_n)]^T$, $\mu_* = [\mu(\mathbf{x}_{1*}), \mu(\mathbf{x}_{2*}), ..., \mu(\mathbf{x}_{n_t*})]^T$, K is n by n matrix whose (i,j) element is $k(\mathbf{x}_i, \mathbf{x}_j)$, K_* is n by n_t matrix whose (i,j) element is $k(\mathbf{x}_i, \mathbf{x}_{j*})$, and K_{**} is n_t by n_t matrix whose (i,j) element is $k(\mathbf{x}_{i*}, \mathbf{x}_{j*})$. Using the useful properties of the Gaussian distribution, the posterior probability distribution can be obtained as follows.

$$\mathbf{f}_* | X, y, X_* \sim \mathcal{N}(\bar{\mathbf{f}}_*, \mathrm{cov}(\mathbf{f}_*)) \tag{9}$$

where

$$\bar{\mathbf{f}}_* = \mathbb{E}[\mathbf{f}_* | X, \mathbf{y}, X_*] = \mu_* + K_*^T K^{-1}(\mathbf{y} - \mu) \tag{10}$$

$$\mathrm{cov}(\mathbf{f}_*) = K_{**} - K_*^T K^{-1} K_* \tag{11}$$

The probability of success can be calculated by integrating the distribution of the posterior latent variables and the link function as

$$\bar{\pi}_{i*} := p(y_{i*} = 1 | X, \mathbf{y}, \mathbf{x}_{i*}, \psi) = \int \sigma(f) p(f | X, \mathbf{y}, \mathbf{x}_{i*}, \psi) df \tag{12}$$

2.4 Laplace approximation

Finding the closed-form expression of the posterior predictive distribution is not analytically tractable. Therefore, the distribution is approximated with the Laplace approximation. Laplace approximation can approximate any posterior distribution as a Gaussian distribution. The approximate Gaussian distribution is obtained using second-order Taylor approximation at the maximum point of the probability distribution function. Let us denote the approximated distribution as

$$q(\mathbf{f}|X,\mathbf{y}) = \mathcal{N}(\mathbf{f};\hat{\mathbf{f}},-(\nabla\nabla^T \log p(\mathbf{f}|X,\mathbf{y})|^{-1}_{\mathbf{f}=\hat{\mathbf{f}}}) =: \mathcal{N}(\mathbf{f},\hat{\mathbf{f}},\hat{\Sigma})) \tag{13}$$

where $\hat{\mathbf{f}} = \text{argmax} p(\mathbf{f}|X,\mathbf{y})$, and $\hat{\Sigma} = -(\nabla\nabla^T \log p(\mathbf{f}|X,\mathbf{y})|^{-1}_{\mathbf{f}=\hat{\mathbf{f}}})$ is the inverse of Hessian of the negative log posterior at that point. The detailed procedure of obtaining $\hat{\mathbf{f}}$ and $\hat{\Sigma}$ can be found in [14]. The posterior expectation and variance for $f_*|X,\mathbf{y},\mathbf{x}_*$ under the Laplace approximation can be expressed as follows,

$$\mathbb{E}_q[f_*|X,\mathbf{y},\mathbf{x}_*] = \mathbf{k}(\mathbf{x}_*)^T K^{-1}\hat{\mathbf{f}} \tag{14}$$

$$\begin{aligned}\mathbb{V}_q[f_*|X,\mathbf{y},\mathbf{x}_*] &= k(\mathbf{x}_*,\mathbf{x}_*) - \mathbf{k}_*^T K^{-1}\mathbf{k}_* + \mathbf{k}_*^T K^{-1}(K^{-1}+W)^{-1}K^{-1}\mathbf{k}_* \\ &= k(\mathbf{x}_*,\mathbf{x}_*) - \mathbf{k}_*^T (K+W^{-1})^{-1}\mathbf{k}_*\end{aligned} \tag{15}$$

Given the expectation and variance, Eqs. (14) and (15), a prediction can be obtained by

$$\bar{\pi}_* \approx \mathbb{E}_q[\pi_*|X,\mathbf{y},\mathbf{x}_*] = \int \sigma(f_*) q(f_*|X,\mathbf{y},\mathbf{x}_*) df_* \tag{16}$$

where $q(f_*|X,\mathbf{y},\mathbf{x}_*)$ is the probability distribution of the posterior latent variable approximated by the Gaussian distribution.

2.5 Hyperparameter tunning

There are multiple hyperparameters in the kernel function in the Gaussian process classification model.. These hyperparameters should be determined appropriately. Hyperparameters can be estimated using given data. Applying the Bayes rule, the posterior distribution of the hyperparameters is expressed as

$$p(\psi|X,\mathbf{y}) = \frac{p(\mathbf{y}|X,\psi)p(\psi)}{\int p(\mathbf{y}|X,\psi)p(\psi)d\psi} \tag{17}$$

where $p(y|X,\psi)$ is marginal likelihood of $\mathbf{y}$, and $p(\psi)$ is prior distribution on the hyperparameters. If there is no prior knowledge of the choice of ψ, the prior distribution of ψ is generally set to be a uniform distribution. The posterior predictive distribution should be marginalized over $p(\psi|X,\mathbf{y})$ as

$$p(\mathbf{f}|X,\mathbf{y},\mathbf{x}_*) = \int p(\mathbf{f}|X,\mathbf{y},\mathbf{x}_*,\psi)p(\psi|X,\mathbf{y})d\psi \tag{18}$$

In practice, the analytic integration of Eq. (18) is generally intractable. Rather than computing full distribution over the hyperparameters, a maximum likelihood estimator is needed in this study, which is computationally tractable. Assuming that the prior distribution of hyperparameters is uniformly distributed, the posterior of the hyperparameter distribution $p(\psi|X,\mathbf{y})$ is proportional to the $p(\mathbf{y}|X,\psi)$.

Therefore, the maximum likelihood estimator can be obtained by maximizing $p(\mathbf{y}|X,\psi)$ for hyperparameters ψ as

$$\psi^* = \underset{\psi}{\operatorname{argmax}}\, p(\mathbf{y}|X,\psi) \tag{19}$$

Note that the optimal value ψ^* can be computed using the conjugate gradient method [15]. Now, the integration of Eq. (18) is replaced with a point estimate at the maximum likelihood values.

2.6 Active sampling

Active sampling is a technique that selects the subset of data from the given data to improve the performance of a given predictive model. Various methods exist according to the criteria for selecting data and the method of sampling the data [13]. Among these methods, the importance-weight random sampling method is adopted in this study. The specific algorithm of the importance-weight random sampling method is as follows. First, the weight is determined according to a predetermined measure. Then, a probability value for each data is allocated based on the determined weight. The probability distribution can be obtained as

$$\mathbb{P}_V(f) = \frac{1}{Z_V} Var(f|X,\mathbf{y},\mathbf{x}) \tag{20}$$

where $Z_V = \sum_{i=1}^{\mathbb{X}_d} Var(f_i|X,\mathbf{y},\mathbf{x}_i)$. The discrete probability distribution is determined from the probability values obtained by Eq. (20). Then, a new dataset is obtained by sampling from the probability distribution. In this way, data with a high weight can be selected with high probability. In addition, data with low weights can be evenly selected, thereby preventing overfitting. The output data is obtained by performing a simulation with the data input obtained. Finally, the obtained input/output data are combined to generate a new dataset. In the importance-weight random sampling method, it is crucial to determine a criterion for appropriate data selection. In this study, the variance value obtained from the predictive model is chosen as the selection criterion. The closer the probability value obtained from the predictive model is to 0.5, the greater the data variance will be. Therefore, it may be expected that the prediction model's performance near the decision boundary will be improved by focusing on collecting data in such regions.

3 Engagement Kinematics

This section describes the missile engagement and guidance law. The engagement kinematic of the missile and target is shown in Fig. 1. V_M, V_T are the speeds of missile and target, respectively, and γ_M, γ_T are the flight path angles of the missile and target, respectively. a_M is the normal acceleration of the missile. The relative position between the missile and target is expressed as a line-of-sight (LOS) angle and a relative distance r. The look angle σ of the missile is expressed as

$$\sigma = \lambda - \gamma_M \tag{21}$$

It is assumed that the angle of attack (AoA) of the missile is small, and the range of the field-of-view is symmetric. That is, $\sigma_{\max} = \sigma_{\lim}$, and $\sigma_{\min} = -\sigma_{\lim}$. The relative nonlinear kinematic equations of the missile and target are expressed in the polar coordinate system as

$$\dot{r} = V_T \cos(\gamma_T - \lambda) - V_M \cos(\gamma_M - \lambda) \tag{22}$$

$$r\dot{\lambda} = V_T \sin(\gamma_T - \lambda) - V_M \sin(\gamma_M - \lambda) \tag{23}$$

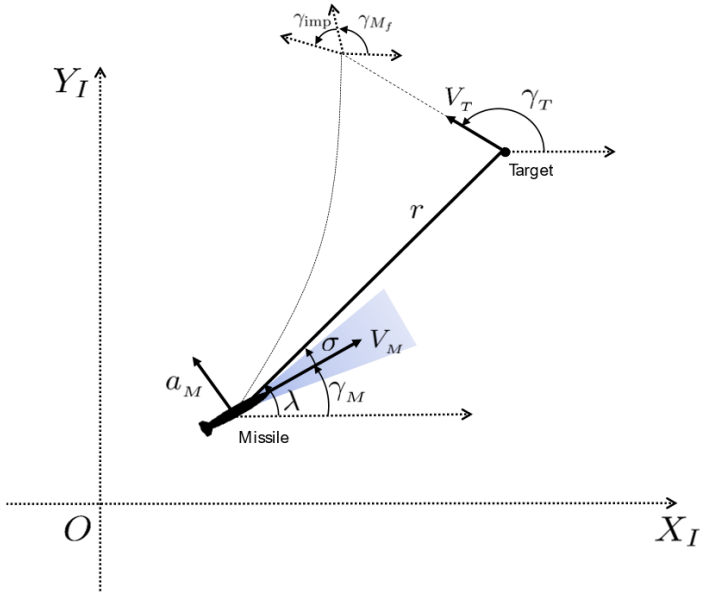

Fig. 1 Planer engagement geometry

$$\dot{\gamma}_M = \frac{a_M}{V_M} \tag{24}$$

In this study, impact-angle control composite guidance (IACCG) law is considered [5]. IACCG is one of the guidance methods that consider the impact angle requirements. In the case of proportional navigation (PN) guidance law the range of impact angles that can be achieved is limited depending on the initial launch location and navigation gain. Therefore, IACCG introduced a deviated pursuit guidance to expand the range of the achievable impact angle while intercepting the targets. IACCG is divided into two stages. First, the deviated pursuit guidance law makes a missile reach a position that can satisfy the impact angle requirement within the range of the missile field-of-view. After that, the target is intercepted while satisfying the impact angle requirement using PN guidance law. The IACCG can be represented as follows,

$$a_M = \begin{cases} V_M\dot{\lambda} + G(\sigma_d - \sigma) & \text{for } |\lambda| < |\lambda_s| \\ NV_M\dot{\lambda} \quad \text{with} \quad N \geq 3 & \text{for } |\lambda| \geq |\lambda_s| \end{cases} \tag{25}$$

$$\lambda_s = \left[\tan^{-1}\left(\frac{\sin\gamma_{M_f} - \eta\sin\gamma_T}{\cos\gamma_{M_f} - \eta\cos\gamma_T}\right) - \frac{\gamma_{M_f} - \sigma_d}{N}\right]\left(\frac{N}{N-1}\right) \tag{26}$$

where γ_{M_f} is the flight path angle of the missile at the interception, $\eta = V_T/V_M$, N is a navigation gain, and σ_d is look angle command. The navigation gain and σ_d should be determined in advance. The navigation gain is set to 3 in this study. According to Ref. [5], it is crutial to set σ_d to meet the conditions. In this study, for the convenience of analysis, the values of the initial look angle and σ_d are set equally. The reason for this setting is not to consider the transient response of the look angle converging to σ_d from the initial value. Therefore, the missile maintains a constant look angle until the guidance law is switched to PN guidance law.

4 Numerical results

Numerical simulations are performed to demonstrate the performance of the proposed method. First, a dataset is generated based on the missile simulator with the initial launch condition as input and the intercept success or failure as output. The generated dataset is divided into a training dataset and a test dataset. The training dataset is used to learn the prediction model, and the test dataset is used to verify the performance of the trained prediction model. In the process of active sampling, the learning process of the model is examined, and the performance of the final model is confirmed. After that, the benefits of active sampling are analyzed by comparing the performance with the learning model that does not use active sampling.

4.1 Given dataset

Data on the accurate capture region is required to evaluate the performance of the proposed algorithm—the reference dataset is generated as follows. IACCG is used as the guidance law. The relative distance between the guided bomb and the target, the LOS angle, and the look angle are the inputs to the dataset, and whether or not the engagement is successful is the output of the dataset. The input of the reference dataset is configured as follows. The relative distance is divided into 250 m intervals between 250 m and 5,000 m. The LOS angle is divided into 1 deg intervals from -40 deg to 40 deg, and the look angle is divided into 1 deg intervals from -45 deg to 45 deg. The data pair is obtained by performing simulations to intercept the target moving at a constant speed of 50 m/s. Finally, a total of 147,240 datasets is collected. There are four conditions for intercept success. If all of the following conditions are satisfied, the intercept is considered successful.

i) The missile does not exceed the field-of-view limit (45 deg) during the engagement.
ii) The maximum acceleration of the missile does not exceed 20 g.
iii) The maximum allowable miss-distance error is within 1 m.
iv) The maximum allowable impact angle error is within 1 deg.

4.2 Simulation setting

Table 1 summarizes the parameters for training. An initial prediction model is needed before active sampling begins. The initial number of data is the number of data used to learn the initial prediction model. Ten data points were uniformly sampled without replacement from the data pool, used to learn the initial prediction model. The batch is the number of data to be sampled during active sampling. Data can be efficiently selected by appropriately setting the number of batches. Twenty data are extracted from the entire learning data and used as batch data at each iteration. Active sampling is repeated 20 times, and as a result, 390 data are used.

Table 1 Training parameters

Parameters	Values
Number of initial data	10
Number of batch	20
Number of iteration	20
Number of test data	14,724

4.3 Training results

Figure 2 shows the accuracy of the prediction model along with the number of data used in training. The accuracy of the prediction model represents a ratio at which the output of the prediction model and

the output of the test data match among the total test data. At the beginning of the training, 100 data are used, and 10 data are added every iteration. Under the same conditions, 100 Monte Carlo simulations were performed, and the mean and standard deviation of the accuracy of the predictive model was shown. The solid blue line shows the average accuracy, and the blue translucent colored area shows the standard deviation. At the beginning of learning, the average accuracy is about 78 %, and the standard deviation is relatively large. It can be seen that as learning progresses, accuracy improves on average, and standard deviation gradually decreases. It can also be confirmed that the average accuracy after 100 repetitive learning converges to a value of about 99.0 %. In addition, as learning progresses, the uncertainty of accuracy gradually decreases. These results show that stable learning is achieved by performing active sampling regardless of the distribution of the initial dataset.

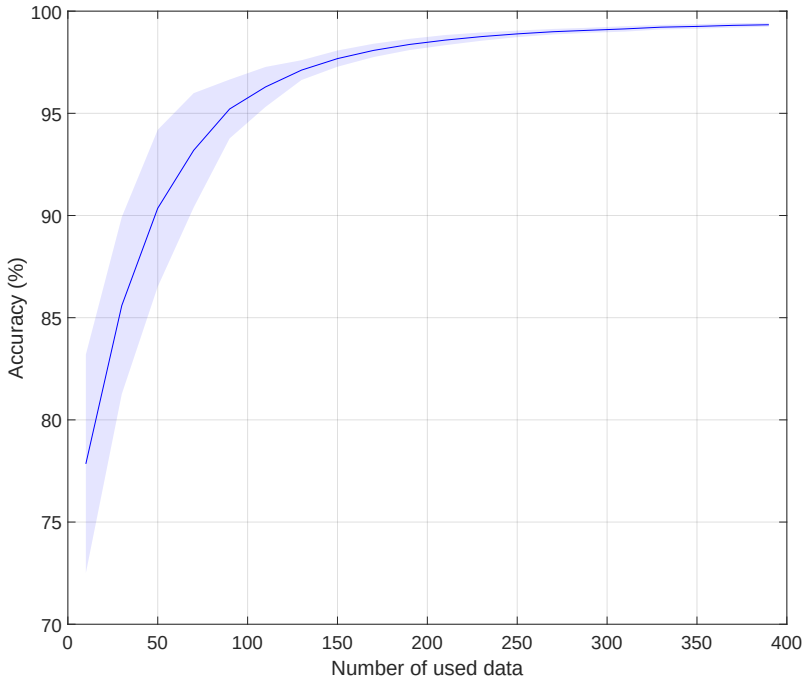

Fig. 2 Accuracy history

Figure 3 shows the change in the capture region predicted by the trained model as the data is gradually added through active sampling. In Fig. 3, only the data with a look angle of 0 are shown in a two-dimensional plane with relative distance and LOS angle as axes because the three-dimensional figure is very complex to understand. The red dot represents the data that failed to intercept, and the blue dot represents the data that succeeded in intercepting. The black line represents the boundary of the capture region estimated by the prediction model, which is called the decision boundary. The decision boundary of the capture region is a contour line in which the output value of the predictive model has a value of 0. As the number of data increases to 140, 190, 240, 290, it can be seen that the decision boundary of the predictive model (black line) divides the success and failure points of the actual data more accurately. These results visually show that the accuracy of the predictive model is improved as training progresses.

The performances of the three differently trained models are also compared. Cases 1 and 2 are the cases in which the model is trained using 1,100 and 3,300 data, respectively, *without active sampling*. Case 3 is the one in which the model is trained using 1,100 data *with active sampling*. Computational time, data usage, and accuracy are used for performance evaluation metrics, which are summarized in Table 2. In Table 2, simulation time is the time obtaining data through a simulator. The total calculation time is the sum of simulation time and training time. It can be seen that the accuracy of Case 2 (99.01 %) is higher than that of Case 1 (98.30%). Compared with Case 1, a more accurate predictive model can be obtained by using more data for training in Case 2. However, the most accurate predictive model

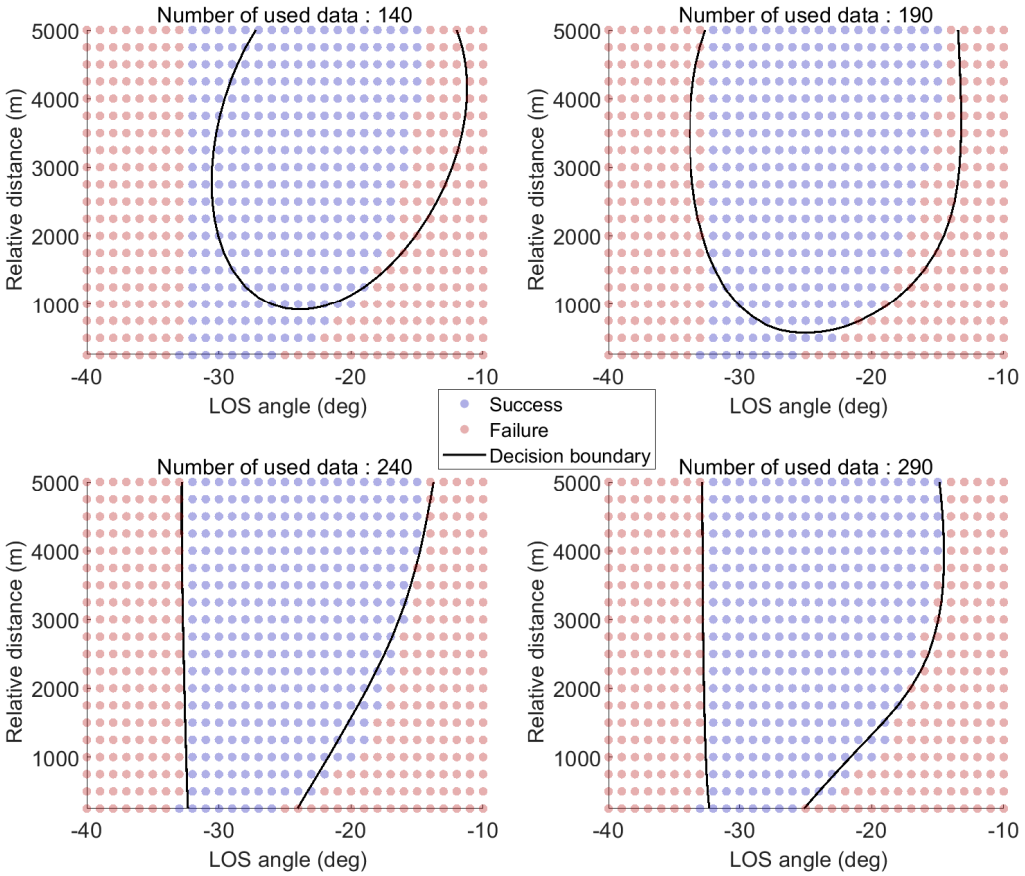

Fig. 3 Evolution of the decision boundary of the predictive model

Table 2 Comparison of performance

	Case 1 (GPC)	Case 2 (GPC)	Case 3 (GPC + AS)
Simulation time (s)	220	660	220
Training time (s)	33	1,320	2,251
Total computation time (s)	253	1,980	2,471
Number of used data	1,100	3,300	1,100
Accuracy (%)	98.30	99.01	99.69

is obtained in Case 3, although it uses the same number of data as in Case 1. This result shows that GPC+AS can efficiently obtain a predictive model with high accuracy using fewer data.

For the training time, Case 3 is the largest at 2,251 seconds. Conducting training several times is the dominant factor for increasing the training time. Due to this effect, the total calculation time for Case 3 amounts to 2,471 seconds, the largest among the three cases. In this study, a relatively simple planar missile simulator was used to verify the performance. In general, the higher the degree of freedom and reliability of the simulator, the more computational resources are required to obtain data. From this point of view, it is crucial to reduce the total number of data generated through numerical simulation. Therefore, active sampling significantly reduces total computation time when creating data using a computationally expensive simulator.

In the case of GPC prediction models that do not use active sampling, they are trained with uniformly sampled data from the entire input space. However, in the case of predictive models using active sampling, data near the boundary of the capture area are actively added, resulting in relatively more data near the boundary. As a result, the prediction model applying the active sampling technique obtains

more information near the boundary, thereby improving the overall prediction performance of the model. According to this analysis, it can be stated that active sampling increases accuracy while efficiently using data. Finally, the proposed method is expected to be one of the alternatives for the Monte Carlo simulation in capture region analysis.

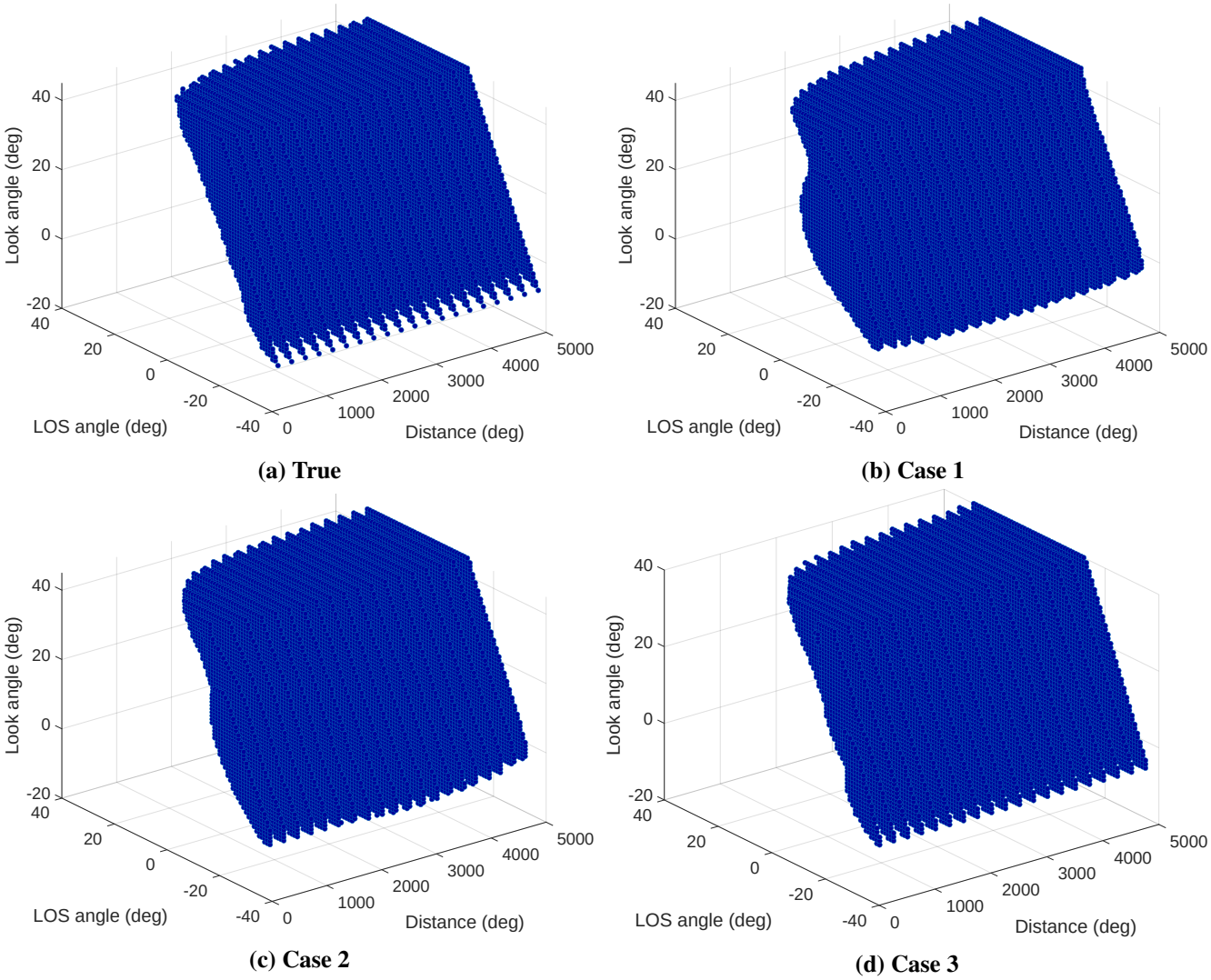

(a) True **(b) Case 1**

(c) Case 2 **(d) Case 3**

Fig. 4 True and estimated capture regions

Figure 4 shows the true and estimated capture regions. Figure 4a) shows the actual three dimensional capture region. Figures 4b), 4c), and 4d) show the capture region estimated by each trained predictive model. Figures 4b), and 4c) are the results of the estimated capture region when the model is trained using 1,100 and 3,300 data without active sampling, respectively (Cases 1 and 2). Figure 4d) shows the results of the estimated capture region with active sampling (Case 3). Comparing Figs. 4b), 4c), and 4d) with the Fig. 4a), it can be seen that the capture region in Fig. 4d) is much more similar to the actual capture region.

5 Conclusion

The methodology of estimating the capture region of missiles was proposed by combining Gaussian process classification and active sampling. It was shown that combining Gaussian process classification with active sampling is a more effective than using Gaussian process classification alone. In general, the capture region depends not only the initial configurations but also on various factors such as flight altitude or speed. In addition, the success of interception can be probabilistic due to aerodynamic uncer-

tainties and disturbances even under the same initial configuration. Future works includes expanding the proposed method considering stochastic factors in a more realistic 3-dimensional engagement scnarios.

Acknowledgments

This work was supported by grants from LIGNex1 Co. Ltd.

References

[1] Bong-Gyun Park, Tae-Hun Kim, and Min-Jea Tahk. Optimal impact angle control guidance law considering the seeker's field-of-view limits. *Journal of Aerospace Engineering*, 227(8):1347–1364, 2013. DOI: 10.1177/0954410012452367.

[2] Namhoon Cho and Youdan Kim. Modified pure proportional navigation guidance law for impact time control. *Journal of Guidance, Control, and Dynamics*, 39(4):852–872, 2016. DOI: 10.2514/1.G001618.

[3] Koray S. Erer and Raziye Tekin. Impact time and angle control based on constrained optimal solutions. *Journal of Guidance, Control, and Dynamics*, 39(10):2448–2454, 2016. DOI: 10.2514/1.G000414.

[4] In-Soo Jeon and Jin-Ik Lee. Impact-time-control guidance law with constraints on seeker look angle. *IEEE Transactions on Aerospace and Electronic Systems*, 53(5):2621–2627, 2017. DOI: 10.1109/TAES.2017.2698837.

[5] Bong-Gyun Park, Hyuck-Hoon Kwon, Yoon-Hwan Kim, and Tae-Hun Kim. Composite guidance scheme for impact angle control against a nonmaneuvering moving target. *Journal of Guidance, Control, and Dynamics*, 39(5):1132–1139, 2016. DOI: 10.2514/1.G001547.

[6] Seokwon Lee, Namhoon Cho, and Youdan Kim. Impact-time-control guidance strategy with a composite structure considering the seeker's field-of-view constraint. *Journal of Guidance, Control, and Dynamics*, 43(8):1566–1574, 2020. DOI: 10.2514/1.G005063.

[7] Dongsoo Cho and H. Jin Kim. Impact angle constrained sliding mode guidance against maneuvering target with unknown acceleration. *IEEE Transactions on Aerospace and Electronic Systems*, 51(2):1310–1323, 2015. DOI: 10.1109/TAES.2015.140358.

[8] Hyeong-Geun Kim and H. Jin Kim. Field-of-view constrained guidance law for a maneuvering target with impact angle control. *IEEE Transactions on Aerospace and Electronic Systems*, 56(6):4794–4983, 2020. DOI: 10.1109/TAES.2020.2996306.

[9] Seokwon Lee, Sungjun Ann, Namhoon Cho, and Youdan Kim. Capturability of guidance laws for interception of nonmaneuvering target with field-of-view limit. *Journal of Guidance, Control, and Dynamics*, 42(4):869–884, 2019. DOI: 10.2514/1.G003860.

[10] Seokwon Lee and Youdan Kim. Capturability of impact-angle control composite guidance law considering field-of-view limit. *IEEE Transactions on Aerospace and Electronic Systems*, 56(2):1077–1093, 2020. DOI: 10.1109/TAES.2019.2925485.

[11] Seonggyun Kim, Park Sanghyuk Park, Jeongho and, Seoungpil Lee, and Kilhun Kim. Computation for launch acceptability region of air-to-surface guided bomb using artificial neural network. *Journal of the Korean Society for Aeronautical and Space Sciences*, 46(4):283–289, 2018.

[12] Lee Seokwon Lee, Suwon and and Youdan Kim. Active sampling-based data-driven reachability verification for proportional navigation guidance law. *IFAC-PapersOnLine*, 52(12), 2019. DOI: 10.1016/j.ifacol.2019.11.060.

[13] John F. Quindlen, Ufuk Topcu, Girish Chowdhary, and Jonathan P. How. Active sampling for closed-loop statistical verification of uncertain nonlinear systems. In *2018 Annual American Control Conference (ACC)*, pages 6259–6265, 2018. DOI: 10.23919/ACC.2018.8431662.

[14] Carl Edward Rasmussen and Christopher K. I. Williams. *Gaussian processes for machine learning.* Adaptive computation and machine learning. MIT Press, Cambridge, massachusetts, 2006.

[15] M. R. Hestenes and E. Stiefel. Methods of conjugate gradients for solving linear systems. *Journal of research of the National Bureau of Standards*, 49:409–436, 1952.